Cell

Short article

Animal and bacterial viruses share conserved mechanisms of immune evasion

Graphical abstract

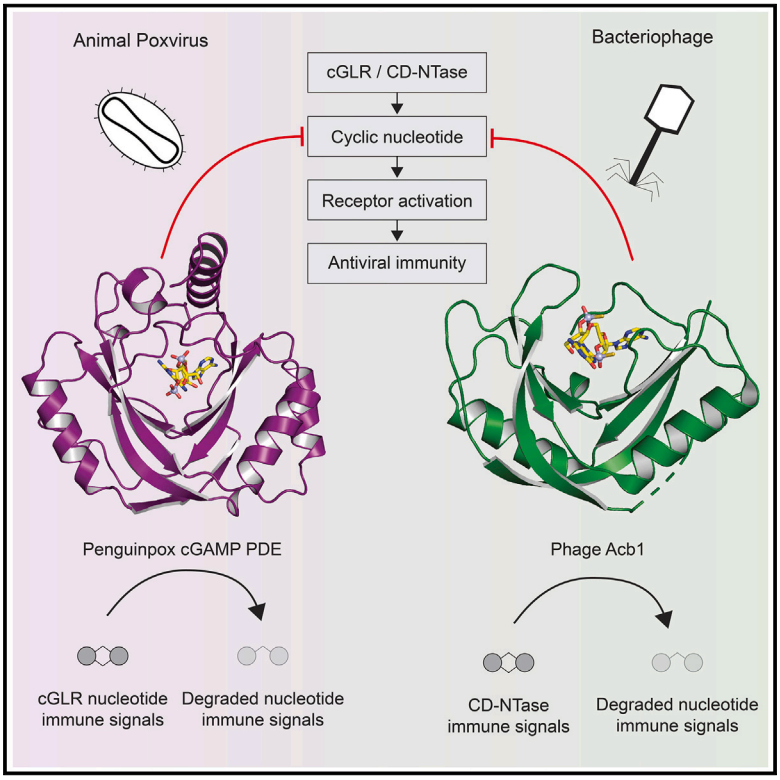

Highlights

- Animal poxviruses encode cGAMP phosphodiesterases that evade host cGLR immunity
- Poxvirus cGAMP PDEs are structurally related to the bacteriophage anti-CBASS protein Acb1
- Poxvirus cGAMP PDE and phage Acb1 use a shared mechanism of cGAMP degradation
- T4 phages encoding poxvirus proteins can overcome bacterial host immunity

Authors

Samuel J. Hobbs, Jason Nomburg, Jennifer A. Doudna, Philip J. Kranzusch

Correspondence

philip_kranzusch@dfci.harvard.edu

In brief

Animal and bacterial cells use related mechanisms of innate immune signaling to restrict viral replication. Here, Hobbs et al. find that poxviruses and bacteriophages use a shared mechanism of immune evasion to overcome conserved host antiviral pathways.

Hobbs et al., 2024, Cell *187*, 5530–5539
October 3, 2024
https://doi.org/10.1016/j.cell.2024.07.057

CellPress

CellPress

Cell

Short article

Animal and bacterial viruses share conserved mechanisms of immune evasion

Samuel J. Hobbs,[1,2] Jason Nomburg,[3,4,5] Jennifer A. Doudna,[3,4,5,6,7,8,9] and Philip J. Kranzusch[1,2,10,*]
[1]Department of Microbiology, Harvard Medical School, Boston, MA 02115, USA
[2]Department of Cancer Immunology and Virology, Dana-Farber Cancer Institute, Boston, MA 02115, USA
[3]Gladstone-UCSF Institute of Data Science and Biotechnology, San Francisco, CA 94158, USA
[4]Department of Molecular and Cell Biology, University of California, Berkeley, Berkeley, CA 94720, USA
[5]Innovative Genomics Institute, University of California, Berkeley, Berkeley, CA 94720, USA
[6]California Institute for Quantitative Biosciences, University of California, Berkeley, Berkeley, CA 94720, USA
[7]Howard Hughes Medical Institute, University of California, Berkeley, Berkeley, CA 94720, USA
[8]Molecular Biophysics and Integrated Bioimaging Division, Lawrence Berkeley National Laboratory, Berkeley, CA 94720, USA
[9]Department of Chemistry, University of California, Berkeley, Berkeley, CA 94720, USA
[10]Lead contact
*Correspondence: philip_kranzusch@dfci.harvard.edu
https://doi.org/10.1016/j.cell.2024.07.057

SUMMARY

Animal and bacterial cells sense and defend against viral infections using evolutionarily conserved antiviral signaling pathways. Here, we show that viruses overcome host signaling using mechanisms of immune evasion that are directly shared across the eukaryotic and prokaryotic kingdoms of life. Structures of animal poxvirus proteins that inhibit host cGAS-STING signaling demonstrate architectural and catalytic active-site homology shared with bacteriophage Acb1 proteins, which inactivate CBASS anti-phage defense. In bacteria, phage Acb1 proteins are viral enzymes that degrade host cyclic nucleotide immune signals. Structural comparisons of poxvirus protein-2′3′-cGAMP and phage Acb1-3′3′-cGAMP complexes reveal a universal mechanism of host nucleotide immune signal degradation and explain kingdom-specific additions that enable viral adaptation. Chimeric bacteriophages confirm that animal poxvirus proteins are sufficient to evade immune signaling in bacteria. Our findings identify a mechanism of immune evasion conserved between animal and bacterial viruses and define shared rules that explain host-virus interactions across multiple kingdoms of life.

INTRODUCTION

Animal, plant, and bacterial cells each require the ability to recognize viral infection and defend against viral replication. Key protein components of antiviral immunity are directly conserved between animal cells and bacteria, demonstrating that the origins of cellular defenses against viral infection are ancient.[1–3] As a founding example, the human cyclic GMP-AMP synthase, stimulator of interferon genes (cGAS-STING) pathway responsible for recognition of viral DNA, originated first in bacteria as an ancient mechanism of anti-phage defense.[4–6] Human cGAS and animal cGAS-like receptors (cGLRs) sense viral nucleic acid and enzymatically synthesize nucleotide immune signals, including 2′–5′, 3′–5′ cyclic GMP-AMP (2′3′-cGAMP), to induce downstream innate immune activation via the receptor STING.[7–11] In bacteria, evolutionarily related cGAS-like enzymes named cGAS/DncV-like nucleotidyltransferases (CD-NTases) sense phage infection and synthesize nucleotide immune signals, including 3′3′-cGAMP, to activate STING-like proteins and other antiviral effectors that induce cell dormancy or cell death to prevent phage propagation.[4–6,12,13] Ancient prokaryotic conservation of proteins in the human interferon response and inflammasome signaling further demonstrate the evolutionary connections that link animal antiviral immunity and bacterial anti-phage defense.[14–18]

Viruses use diverse mechanisms of immune evasion to overcome host antiviral responses. To limit immune recognition, viral replication rapidly selects genome mutations and protein amino acid substitutions that prevent interaction with immune proteins and shield escape viruses from detection.[19–22] In addition to escape mutations, viruses that infect animal and bacterial cells acquire proteins dedicated to inhibition of host immune signaling. Major themes of active immune evasion include viral proteins that directly bind and inhibit host immune receptors,[23–26] viral proteins that degrade host components and signaling molecules,[27–29] and viral replication factors that reprogram cell signaling and metabolism to subvert immune responses.[2,3,30–32] Comparative analyses of viral replication strategies have revealed disparate mechanisms used to inhibit host immunity, but no evolutionary links were thought to directly unite animal and bacterial viral immune evasion.

Here, we show that animal and bacterial viruses share conserved mechanisms of host immune evasion. We find that

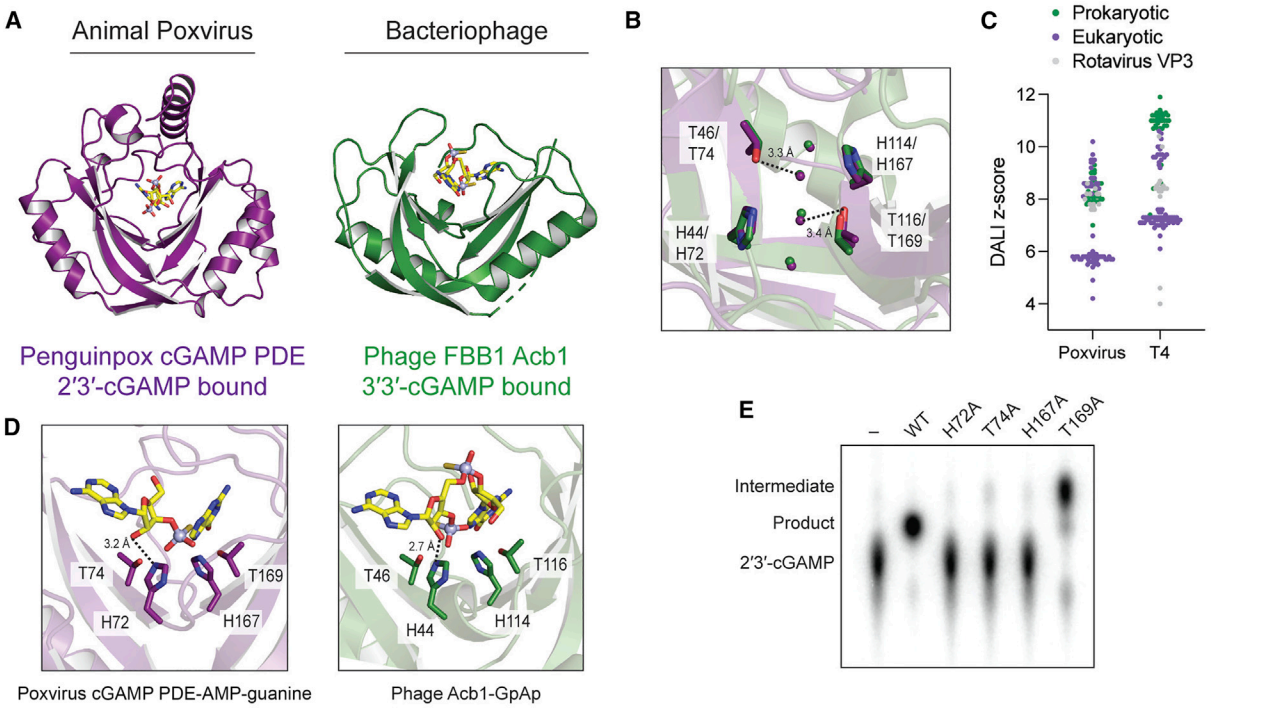

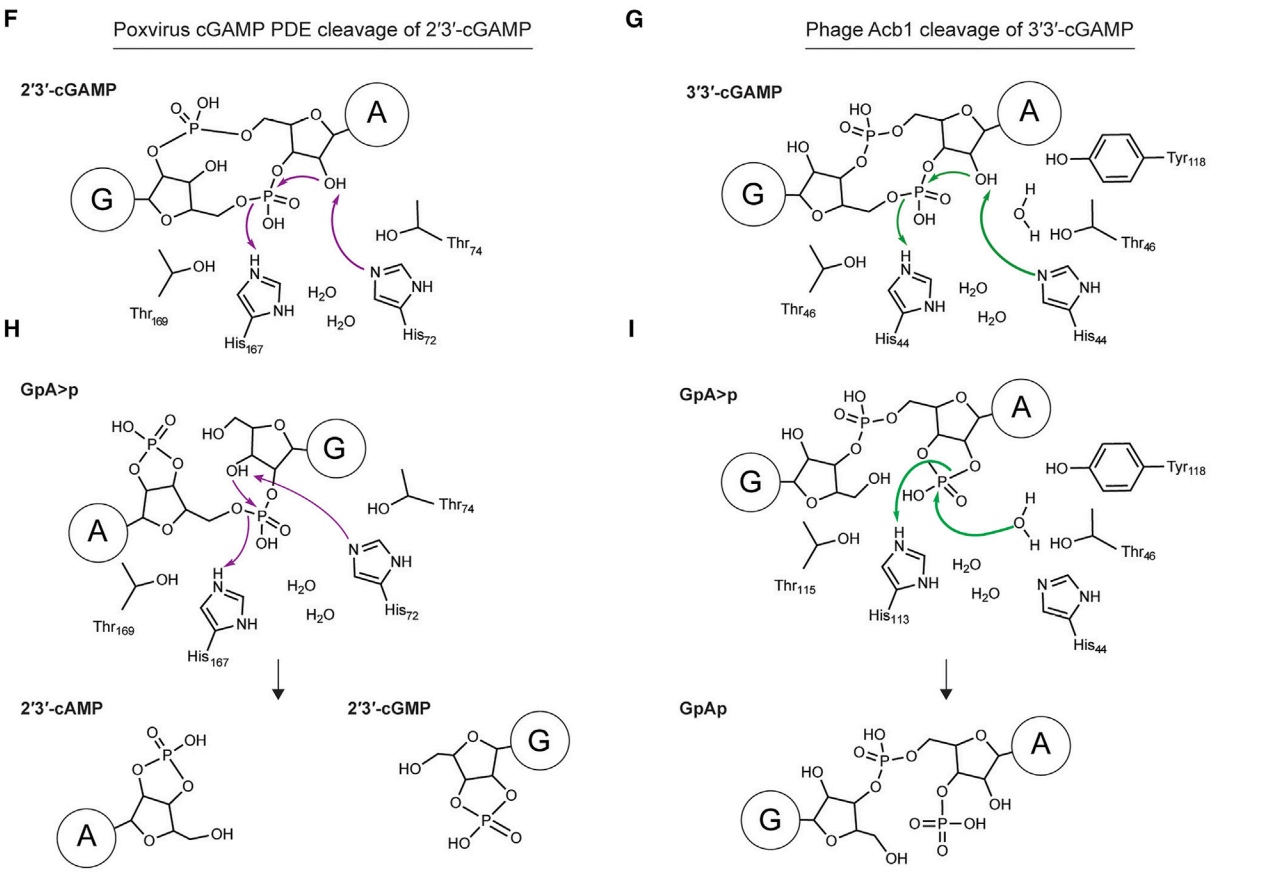

(legend on next page)

animal poxvirus proteins inhibit host cGAS-STING signaling in a manner that is structurally and mechanistically similar to bacteriophage immune evasion proteins that inactivate evolutionarily related cyclic oligonucleotide-based antiviral signaling system (CBASS) defense pathways in bacteria. X-ray crystal structures of poxvirus proteins and phage anti-CBASS (Acb) immune evasion proteins demonstrate that animal and bacterial viral inhibitors share a universal mechanism of host immune signal degradation that prevents animal 2′3′-cGAMP and bacterial 3′3′-cGAMP immune activation. We define kingdom-specific protein additions that repurpose ubiquitous host enzymes for viral immune evasion and demonstrate that evolutionarily related eukaryotic viral immune evasion proteins are sufficient to disrupt immune signaling in bacteria. Our results extend the cross-kingdom conservation of antiviral immunity to include mechanisms of viral immune evasion and define shared rules that explain host-virus interactions across kingdoms of life.

RESULTS

Animal poxvirus proteins are structural and functional homologs of bacteriophage Acb1 immune evasion enzymes

A recent database of protein structure predictions encompassing 4,000 eukaryotic viral species identified uncharacterized proteins in viruses of the family *Poxviridae* as potential homologs of the phage protein Acb1.[33] In bacteria, Acb1 is a phage immune evasion protein that enzymatically degrades nucleotide immune signals to inhibit host CBASS anti-phage defense.[28] To define the relationship between animal poxvirus proteins and phage Acb1, we determined an X-ray crystal structure of a candidate homolog gp029 encoded by penguinpox virus (YP_009046028.1, renamed here "cGAMP phosphodiesterase [PDE]") (Table S1).[34] The structure of poxvirus cGAMP PDE reveals remarkable similarity with phage Acb1 proteins, demonstrating near exact placement of all major structural elements including strands β1–β5 that form a cup-shaped enzymatic core and helices α4, α7, and α8 that brace the outside of the viral enzyme (Figure 1A). Further supporting direct structural similarity, poxvirus cGAMP PDE and phage Acb1 share an identical active-site tetrad comprised of two HxT motifs located on adjacent strands β2 and β4, and each enzyme coordinates a superimposable configuration of four water molecules known to be required for nucleotide substrate coordination (Figure 1B).[28,35] Structural alignment with all experimental structures in the Protein Data Bank (PDB) demonstrates that the catalytic cores of poxvirus cGAMP PDE and phage Acb1 are most similar to 2H phosphoesterase enzymes from their respective host domains, suggesting these viral proteins likely do not share a common origin (Figure 1C).[36]

To define the poxvirus cGAMP PDE reaction mechanism, we crystallized the wild-type (WT) poxvirus cGAMP PDE protein in complex with a hydrolysis-resistant analog of the metazoan nucleotide immune signal 2′3′-cGAMP and a catalytically inactive poxvirus cGAMP PDE mutant (H72A) in complex with 2′3′-cGAMP (Figures 1A and S1A–S1E; Table S1). The poxvirus cGAMP PDE crystallographic asymmetric unit contains two copies of the protein in complex with a partially degraded nucleotide immune signal and two copies of the protein in an unliganded apo state (Figure S1A). Strong electron density in the WT poxvirus cGAMP PDE active site allowed unambiguous modeling of the reaction products adenosine monophosphate (3′-AMP) and a guanine nucleobase consistent with 2′3′-cGAMP cleavage (Figures S1B and S1C). In the H72A mutant structure, strong electron density was observed for G[3′–5′]pA in the binding pocket but poor density for the opposing phosphodiester linkage, suggesting flexibility in the A[2′–5′]pG bond (Figures S1D and S1E). The organization of the poxvirus cGAMP PDE catalytic center and positioning of the reaction products are nearly identical (root-mean-square deviation [RMSD] = 0.231) to previous structures of phage Acb1 in complex with the bacterial nucleotide immune signal 3′3′-cGAMP (Figure 1D). We analyzed the impact of mutations to conserved poxvirus cGAMP PDE catalytic residues using thin-layer chromatography and observed loss of 2′3′-cGAMP cleavage activity, except for T169A, which resulted in the formation of an intermediate cleavage product (Figure 1E). These results mirror the effect of mutating equivalent residues in phage Acb1[28] and suggest a conserved catalytic mechanism used to degrade nucleotide immune signals. We next incubated purified poxvirus cGAMP PDE and phage Acb1 proteins with 2′3′-cGAMP and 3′3′-cGAMP and monitored a time course of degradation using high-performance liquid chromatography (HPLC). Poxvirus cGAMP PDE and phage Acb1

Figure 1. Animal poxvirus cGAMP PDE proteins are structural and functional homologs of bacteriophage Acb1 immune evasion enzymes

(A) Overview of the crystal structure of penguinpox cGAMP PDE in complex with 2′3′-cGAMP degradation products 3′-AMP and guanine (left). Overview of the crystal structure of bacteriophage FBB1 Acb1 in complex with the 3′3′-cGAMP degradation product GpAp (right).

(B) Detailed view of the aligned catalytic residues of either animal poxvirus cGAMP PDE (purple) or phage Acb1 (green). Spheres represent water molecules coordinated between catalytic residues.

(C) DALI *Z* scores of poxvirus cGAMP PDE and phage Acb1 when searched against all structures in the PDB. Hits from eukaryotic organisms are colored purple; hits from prokaryotic organisms are colored green; and hits to rotavirus VP3 proteins are colored gray.

(D) Detailed view of the active site of poxvirus cGAMP PDE bound to the reaction product 3′-AMP (left) or the active site of phage Acb1 bound to the reaction product GpAp (right).

(E) Thin-layer chromatography of radiolabeled 2′3′-cGAMP treated with poxvirus cGAMP PDE with the indicated mutations.

(F) Detailed mechanism of the first step of 2′3′-cGAMP cleavage by poxvirus cGAMP PDE.

(G) Detailed mechanism of the first step of 3′3′-cGAMP cleavage by phage Acb1.

(H) Proposed mechanism of the second step of poxvirus cGAMP PDE cleavage of GpA>p to form the cyclic mononucleotide products 2′3′-cGMP and 2′3′-cAMP.

(I) Proposed mechanism of the second step of phage Acb1 cleavage of Gp[3′–5′]A>p to form the linear dinucleotide product Gp[3′–5′]A[3′]p (right). Note that the nucleophilic water molecule is not one of the highly conserved four active-site water molecules.

See also Figure S1.

rapidly hydrolyze cGAMP species to produce a linear intermediate product with a terminal 2′3′ cyclic phosphate (G[2′–5′]pA[2′–3′]>p and G[3′–5′]pA[2′–3′]>p) consistent with attack of the scissile phosphate by the 2′ hydroxyl group of adenosine (Figures 1F, 1G, S1F, and S1G). Following the formation of this intermediate, poxvirus cGAMP PDE further cleaves the product to form cyclic mononucleotides species 2′3′-cAMP and 2′3′-cGMP, whereas phage Acb1 hydrolyzes the terminal 2′–3′ cyclic phosphate to form the linear dinucleotide product G[3′–5′]pA[3′]p, suggesting differences in enzyme nucleobase preference (see below) (Figures 1H, 1I, S1F, and S1G). Together, these results demonstrate that eukaryotic viral poxvirus cGAMP PDE and prokaryotic viral phage Acb1 enzymes are members of a single family of immune evasion proteins that target host nucleotide immune signals across domains of life.

Poxvirus cGAMP PDE and phage Acb1 proteins require a lid domain to target host nucleotide immune signals

Animal and bacterial nucleotide immune signals, including 2′3′-cGAMP and 3′3′-cGAMP, are normally highly refractory to enzymatic degradation. Due to the small size and restrained cyclic phosphodiester backbone, these molecules are resistant to degradation by cellular nucleases that process normal cellular nucleic acid.[27] In phage immune evasion, inhibition of 3′3′-cGAMP signaling is enabled by an Acb1 C-terminal lid domain that closes over the active site and allows capture and degradation of host CBASS nucleotide immune signals.[28] In poxvirus cGAMP PDE, the lid domain is absent from the protein C terminus and is instead formed by a large structural addition of a 20-residue alpha helix (α1′) at the N terminus of the animal viral protein (Figure 2A). Deletion mutants confirm that the lid regions of poxvirus cGAMP PDE and phage Acb1 are each required for degradation of 2′3′-cGAMP and 3′3′-cGAMP (Figure 2B). Upon 2′3′-cGAMP binding, the poxvirus cGAMP PDE N-terminal lid rotates sideways ∼25° over the active site and positions residue F155 within an intervening loop to form pi-stacking interactions with the guanine nucleobase of the captured substrate (Figure 2C). Poxvirus cGAMP PDE residue Y63 forms an additional pi-stacking interaction with the adenine nucleobase over a hydrophobic platform containing residues I77 and L25 (Figure 2C). The resulting interactions twist the bound nucleotide immune signal into a highly strained conformation in which the target nucleobase is rotated ∼50° relative to in-solution and receptor-bound nucleotide immune signal conformations, enabling attack of the 2′ OH group on the scissile phosphate (Figure 2D).[37,38] The mechanism of poxvirus cGAMP PDE 2′3′-cGAMP capture results in a near identical substrate configuration observed in previous structures of phage Acb1 (Figure 2E). An aromatic residue W147 in the C-terminal lid of phage Acb1 similarly forms stacking interactions with the adenine nucleobase of 3′3′-cGAMP, highlighting a shared molecular strategy to target and degrade eukaryotic and bacterial host nucleotide immune signals.

Poxvirus cGAMP PDE proteins target diverse nucleotide immune signals and enable cross-kingdom evasion of host immunity

Animal cGLR and bacterial CD-NTase enzymes synthesize a wide array of nucleotide immune signals that control host antiviral immune responses. Distinct cGLR and CD-NTase products include the formation of cyclic di- and trinucleotide compounds, incorporation of purine and pyrimidine nucleobases, and use of 3′–5′ and 2′–5′ phosphodiester bonds.[4,11,12] To define the ability of viruses to inhibit diverse host immune signaling pathways, we measured the activity of poxvirus cGAMP PDE and phage Acb1 enzymes against a panel of nucleotide immune signals, including common examples in animal innate immunity (2′3′-cGAMP, 3′2′-cGAMP, 2′3′-cGG, 3′3′-cAA), bacterial anti-phage defense (3′3′-cGAMP, 3′3′-cGG, 3′3′3′-cAAA), and bacterial signaling (3′3′-cGG, 3′3′-cAA) (Figure 3A).[4–8,10,11,39–42] Poxvirus cGAMP PDE and phage Acb1 are capable of degrading nearly all tested nucleotide immune signals (Figure 3B). Notably, poxvirus cGAMP PDE most efficiently degraded animal nucleotide immune signals (2′3′-cGAMP, 3′2′-cGAMP, 2′3′-cGG) and phage Acb1 most efficiently degraded bacterial nucleotide immune signals (3′3′-cGAMP and 3′3′3′-cAAA), supporting enzyme specialization for evasion of kingdom-specific host antiviral pathways (Figure 3B). In further support of kingdom-specific adaptation, poxvirus cGAMP PDE efficiently degrades 3′3′-cGG, but phage Acb1 specifically avoids degradation of 3′3′-cGG as this cyclic dinucleotide is rarely used in anti-phage defense and is instead required for normal bacterial cell function (Figure 3B).[43]

In animal immunity, the fruit fly *Drosophila melanogaster* has emerged as a key model for studying the function of animal cGLR enzymes in host-virus interactions.[39–41] We therefore analyzed the database of predicted eukaryotic viral protein structures for cGAMP PDE representatives from *Drosophila* viruses and identified a candidate protein 127L from the *Drosophila* DNA virus invertebrate iridescent virus 6 (IIV-6) (NP_149590.1, renamed here cGAMP PDE) (Figure 3A).[33,44] IIV-6 cGAMP PDE encodes an intact HxT catalytic tetrad and contains an ∼18 residue N-terminal extension lid domain similar to poxvirus cGAMP PDE. We purified IIV-6 cGAMP PDE and observed that this enzyme degrades the *Drosophila* nucleotide immune signals 2′3′-cGAMP and 3′2′-cGAMP but fails to cleave prokaryotic nucleotide immune signals, including 3′3′-cGAMP (Figure 3B). Phage Acb1 and poxvirus cGAMP PDE both largely depend on non-specific base-stacking interactions to bind 3′3′-cGAMP and 2′3′-cGAMP. Based on the predicted AlphaFold structure, IIV-6 cGAMP PDE similarly encodes aromatic residues in equivalent positions, suggesting that non-specific stacking interactions are a universal feature of viral cGAMP PDEs that enable targeting of multiple cyclic nucleotide substrates (Figure S2A). Some insect DNA and RNA viruses encode poxin (poxvirus immune nuclease) proteins that degrade 2′3′-cGAMP.[27,45] The *Drosophila* nucleotide immune signal 3′2′-cGAMP is resistant to poxin enzymes, suggesting nucleotide variation is a counter-defense mechanism host animals use to restore antiviral signaling.[39] As animal hosts diversify signaling pathways beyond 2′3′-cGAMP, the broader ability of poxvirus cGAMP PDE and IIV-6 cGAMP PDE enzymes to target 3′2′-cGAMP and related nucleotide immune signals may therefore provide an evolutionary advantage to resisting host antiviral immunity.

To identify additional candidate eukaryotic viral cGAMP PDE enzymes that may target cyclic nucleotide immune signals, we performed structural alignments of a panel of predicted and

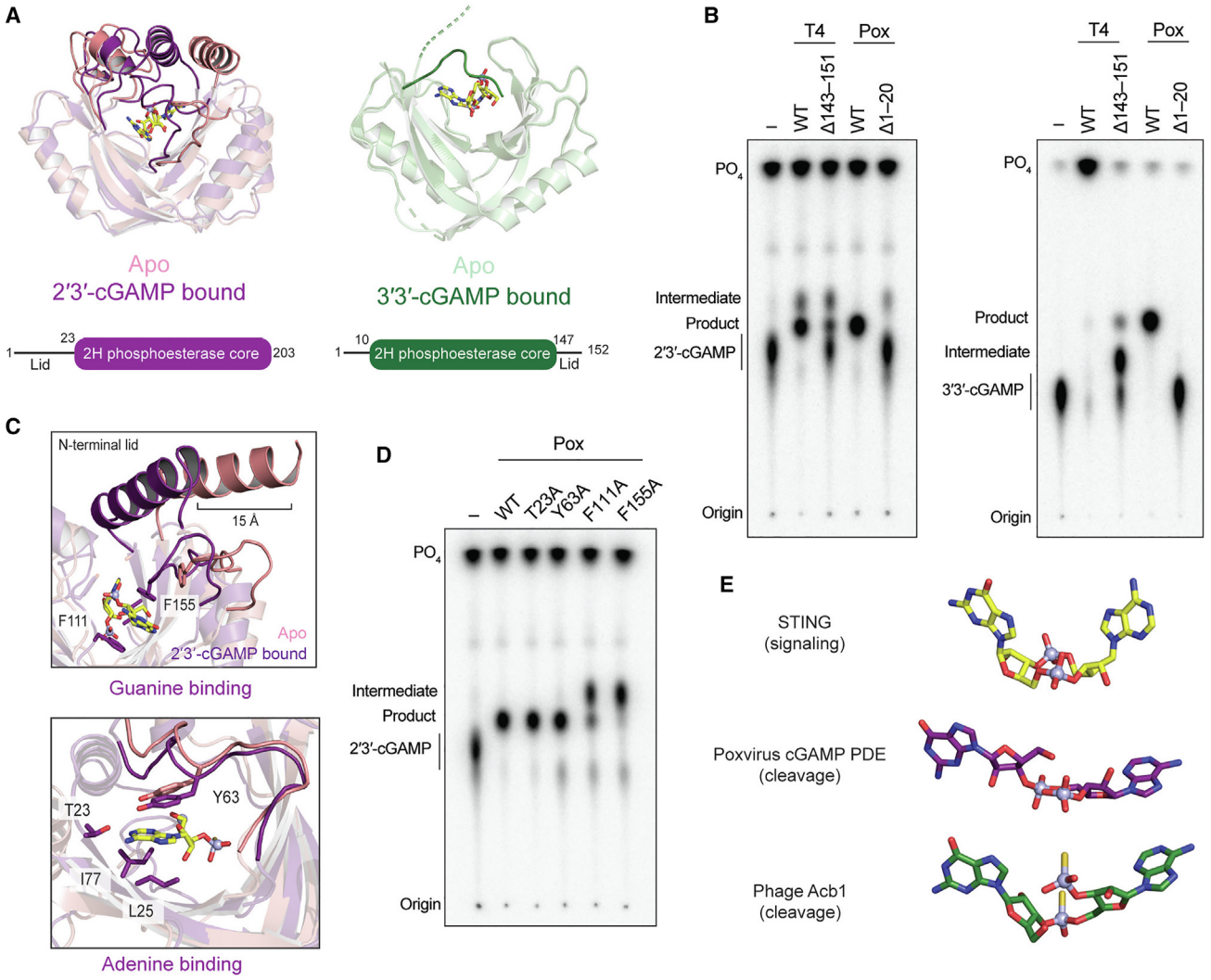

Figure 2. Poxvirus cGAMP PDE and phage Acb1 lid domains enable targeting of host nucleotide immune signals

(A) Overview of the domain structure and apo and 2′3′-cGAMP-bound structures of poxvirus cGAMP PDE (left). Overview of the domain structure and apo and 2′3′-cGAMP-bound structures of poxvirus cGAMP PDE (right). Lid domains are highlighted in both structures.

(B) Thin-layer chromatography of radiolabeled 2′3′-cGAMP or 3′3′-cGAMP treated with WT or lid domain deletion mutants of poxvirus cGAMP PDE or phage Acb1.

(C) Detailed view of the N-terminal lid movement and residues involved ligand binding in poxvirus cGAMP PDE.

(D) Thin-layer chromatography of radiolabeled 2′3′-cGAMP treated with poxvirus cGAMP PDE with the indicated mutations.

(E) Comparison of the conformation of 3′3′-cGAMP bound to the receptor STING (PDB: 5CFM), cleaved 2′3′-cGAMP from poxvirus cGAMP PDE structure, and cleaved 3′3′-cGAMP from phage Acb1 (PDB: 7T27).

See also Figure S2.

experimental structures of eukaryotic viral and phage 2H phosphoesterase enzymes. A hypothetical protein from Marseillevirus (ORF259, GenBank: YP_003406995.1) exhibits significant structural similarity to IIV-6 cGAMP PDE and encodes an analogous N-terminal lid domain (Figure S2B), suggesting that cGAMP PDE enzymes may be relatively conserved in the order *Pimascovirales*. Middle East Respiratory Syncitial virus (MERS) protein NS4B (GenBank: YP_009047207.1) and porcine torovirus polyprotein 1a are more distantly related to Penguinpox and IIV-6 cGAMP PDE enzymes but encode either an N-terminal extension or are part of a polyprotein that could potentially function as a lid (Figure S2B).

We next asked whether the ability of viral enzymes to target diverse nucleotide immune signals is sufficient to allow cross-kingdom evasion of host immunity. To test cross-kingdom immune evasion, we sought to engineer a recombinant phage T4 virus where the *acb1* gene is replaced with the animal viral poxvirus cGAMP PDE. In addition to Acb1, T4 also encodes another Acb protein Acb2 that functions as a sponge to sequester 3′3′-cGAMP and prevent CBASS immune activation.[25,46] We therefore first

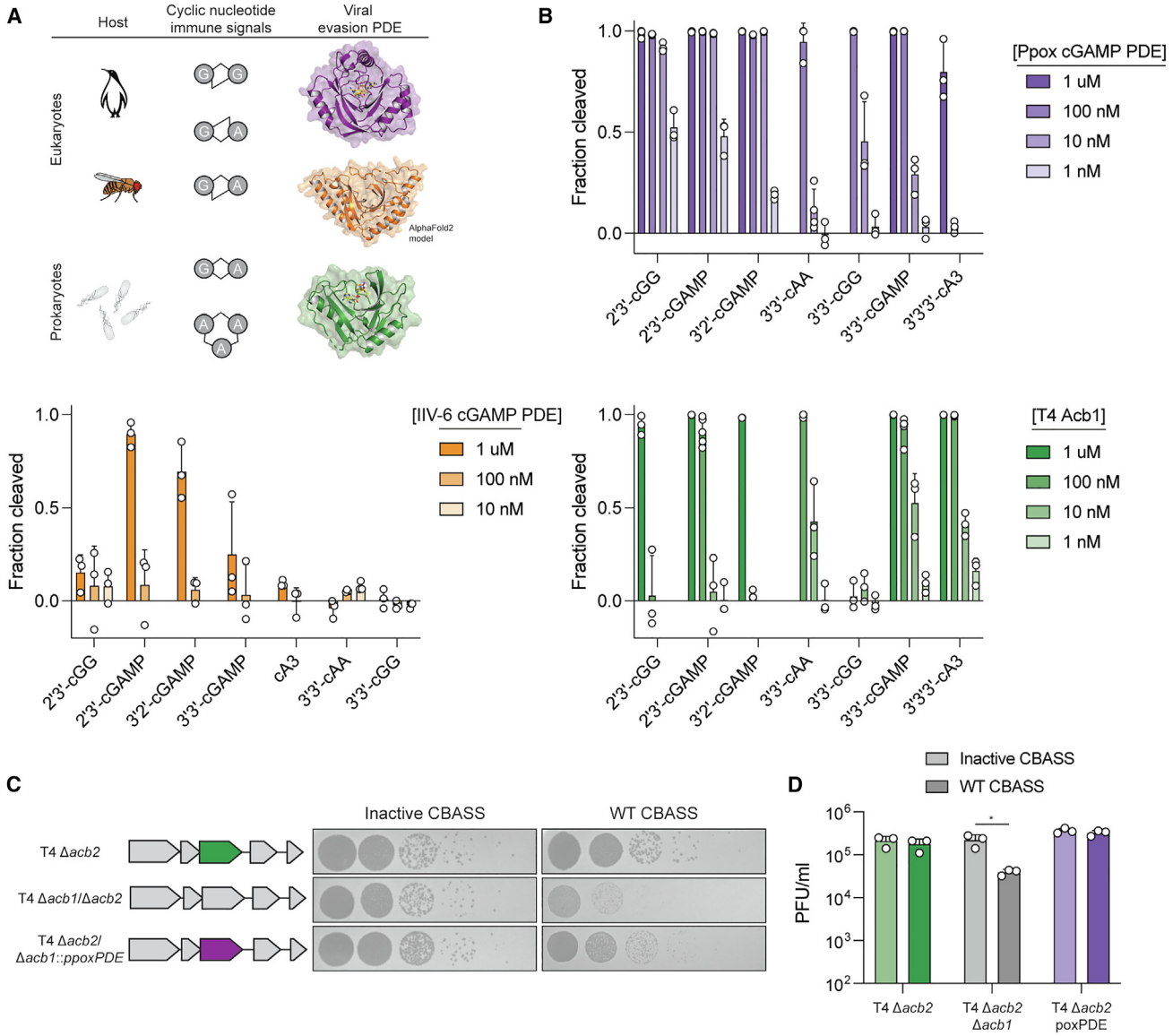

Figure 3. Eukaryotic Acb1 proteins target diverse host nucleotide immune signals and enable phage evasion of CBASS immunity

(A) Overview of common nucleotide immune signals used in eukaryotic and prokaryotic immunity. Included in this table is the predicted structure of a putative cGAMP PDE from the *Drosophila* virus invertebrate iridescent virus 6 (IIV-6) identified by the presence of an N-terminal lid over the 2H phosphoesterase active site in the AlphaFold2 prediction. Error bars represent one standard deviation.

(B) Summary of cleavage activity of poxvirus cGAMP PDE, *Drosophila* cGAMP PDE, and phage Acb1 against a panel of nucleotide immune signals primarily used in either eukaryotes or prokaryotes.

(C) Representative images of the plaque assays using the indicated mutant T4 phages plated on *E. coli* expressing either an active or inactive CBASS operon.

(D) Quantification of the data in (C). Significance was determined using an unpaired t test and a p value of less than 0.05. Error bars represent one standard deviation.

See also Figure S3.

generated a phage T4 Δ*acb2* knockout parental strain, which we then used to construct a series of phage T4 variants encoding either endogenous *acb1* (T4 Δ*acb2*), a non-functional *acb1* (T4 Δ*acb2*/Δ*acb1*), or endogenous *acb1* replaced with penguinpox cGAMP PDE (T4 Δ*acb2*/Δ*acb1::pox*) (Figure 3C). Sequencing confirmed successful construction of each phage T4 variant (Figure S3A). Lysates from T4 Δ*acb2*/Δ*acb1::pox* infected cells efficiently cleaved 3′3′-cGAMP, demonstrating that the animal protein poxvirus cGAMP PDE is functional during phage infection in bacteria (Figure S3B). We then tested viral fitness in cells encoding a CBASS operon from *Escherichia albertii* that signals using 3′3′-cGAMP.[47,48] In the absence of CBASS immunity, all phage T4 variants replicated equally well and exhibited no loss of viral fitness (Figures 3C and 3D). Replication of the phage T4 virus

lacking Acb1 (T4 Δ*acb2*/Δ*acb1*) was specifically reduced in the presence of active CBASS anti-phage defense (Figures 3C and 3D). By contrast, phage T4 variants expressing Acb1 or the animal poxvirus cGAMP PDE protein efficiently evaded CBASS anti-phage defense, demonstrating that poxvirus cGAMP PDE is sufficient to overcome bacterial nucleotide immune signaling (Figures 3C and 3D). These results demonstrate that an animal viral protein can inhibit bacterial anti-phage defense and highlight Acb1/cGAMP PDE-mediated viral degradation of nucleotide immune signals as a strategy of immune evasion shared across the prokaryotic and eukaryotic kingdoms of life.

DISCUSSION

Our results reveal cGAMP PDE and Acb1 enzymes as a family of immune evasion proteins conserved between eukaryotic viruses and prokaryotic phages. In response to viral infection, animal and bacterial immune pathways can synthesize diverse nucleotide immune signals to activate antiviral immunity and limit viral replication. Animal virus cGAMP PDE and phage Acb1 enzymes degrade these nucleotide immune signals and inhibit host immune activation. Our results extend the recent discovery of immune pathways conserved between animal cells and bacteria[1–3] and demonstrate conservation of viral strategies that defeat host immunity.

Eukaryotic viral cGAMP PDE and prokaryotic phage Acb1 proteins evade host immune signaling using a conserved set of shared molecular features. First, cGAMP PDE/Acb1 proteins adopt the same phosphoesterase catalytic core architecture braced with a set of three conserved helices that creates a compact active site and allows targeting of the small, specialized nucleotide products that control host antiviral immunity (Figure 1). cGAMP PDE/Acb1 proteins form a subset of the 2H phosphoesterase enzyme superfamily that is widespread in all domains of life and contains other notable viral proteins, including rotavirus VP3, coronavirus ns2, and coronavirus NS4b.[36,49,50] Rotavirus VP3 and coronavirus ns2 and NS4b proteins degrade the linear 2′-5′ linked oligoadenylate chains produced by animal oligoadenylate synthase-family immune proteins,[51–53] demonstrating additional forms of 2H phosphoesterase enzymes also used by viruses to disrupt host immune signaling. Second, cGAMP PDE/Acb1 proteins share conserved use of a protein lid domain that enables nucleotide immune signal capture and degradation. Compared with phage Acb1 proteins, crystal structures of the poxvirus cGAMP PDE lid domain reveal an elaborate extension that arises from the opposite protein terminus, suggesting that lid domain variation may contribute to kingdom-specific adaptations that fine-tune viral activity against the nucleotide immune signals prevalent in eukaryotic innate immunity (Figure 2). The distinct size and position of the poxvirus cGAMP PDE and phage Acb1 lid domains suggest that these enzymes are likely the result of convergent evolution. Use of a lid domain is a feature of cGAMP PDE/Acb1 proteins not shared with more distantly related 2H phosphoesterase enzymes, including VP3, ns2, and typical LigT-family bacterial and cyclic nucleotide phosphoesterase-family animal host proteins, explaining why cGAMP PDE/Acb1 proteins are uniquely able to degrade cyclic nucleotide immune signals, including 2′3′-cGAMP.[33,54–56] Finally, cGAMP PDE/Acb1 proteins share an identical metal-independent mechanism to target cyclic phosphodiester linkages used in host nucleotide immune signals. The active site of cGAMP PDE/Acb1 proteins twist nucleotide immune signals into a strained conformation that allows for in-line attack and phosphodiester bond hydrolysis (Figures 1 and 2). Both eukaryotic and prokaryotic viral enzymes degrade host cGAMP molecules into a linear intermediate product that is unable to direct downstream immune activation. Our results with engineered phage T4 variants demonstrate that viral proteins are sufficient to inhibit signaling across kingdoms of life (Figure 3), explaining how transfer of immune evasion proteins may further enable viral resistance to host immunity.

The seminal discovery by Nomburg et al. of sequences in animal poxviruses with predicted similarity to phage Acb1 proteins highlights the importance of large-scale protein structure prediction methods and creation of open-access databases.[33] Continued advances in protein structure prediction[57,58] and genomic databases[59,60] create a rich opportunity to discover additional viral immune evasion proteins conserved across the eukaryotic and prokaryotic domains of life. In the bacterial kingdom, multiple phage proteins have been shown to specifically inhibit nucleotide immune signaling[23–26,29] suggesting eukaryotic viruses may share additional classes of conserved immune evasion proteins dedicated to inhibition of animal cGAS-STING and cGLR signaling pathways. Our analysis of poxvirus cGAMP PDE defines the structural and biochemical features viral enzymes use to target cyclic nucleotides and enables identification of additional enzymes in *Drosophila* viruses that degrade 2′3′-cGAMP. This approach highlights the utility of combining detailed mechanistic studies with structure-guided homology searches to identify viral immune evasion proteins. Taken together, our results highlight a fundamental mechanism of immune evasion and expand the cross-kingdom conservation of animal and bacterial immunity to include viral immune evasion strategies.

Limitations of the study

Our study has identified a conserved mechanism of immune evasion employed by eukaryotic viruses and phages. Using structural and biochemical analyses, we demonstrate that poxvirus cGAMP PDE and phage Acb1 immune evasion proteins share a 2H phosphoesterase enzymatic core and conserved mechanism of nucleotide immune signal degradation, but we are not able to explicitly determine the evolutionary relationship between these viral enzymes. Based on the differences in composition and location of the lid domains, we hypothesize that poxvirus cGAMP PDE and phage Acb1 are a result of convergent evolution. Future studies further characterizing the diversity of viruses encoding related cGAMP PDE enzymes may uncover evolutionary intermediates or additional evidence to support possible direct evolution from a common viral enzyme. Additionally, our biochemical analyses demonstrate that poxvirus cGAMP PDE completely degrades 2′3′-cGAMP into the mononucleotide products 2′3′-cAMP and 2′3′-cGMP. We hypothesize that poxvirus cGAMP PDE releases the linear dinucleotide intermediate following cleavage of the 3′–5′ bond downstream of

adenine and re-binds the intermediate in the opposite orientation with the 2′–5′ bond downstream of guanine oriented toward the active-site residues (Figures 1F and 1H). However, our data do not formally exclude the possibility that residues in the poxvirus PDE lid domain participate in direct cleavage of the 2′–5′ bond. Finally, studies defining the role of poxvirus cGAMP PDE enzymes during infection will be critical to understanding the function of these proteins *in vivo* and the evolutionary pressures that dictate which nucleotide immune signals are targeted.

STAR★METHODS

Detailed methods are provided in the online version of this paper and include the following:

- KEY RESOURCES TABLE
- RESOURCE AVAILABILITY
  - Lead contact
  - Materials availability
  - Data and code availability
- EXPERIMENTAL MODEL AND STUDY PARTICIPANT DETAILS
- METHOD DETAILS
  - Cloning and plasmid construction
  - Protein expression and purification
  - Crystallization and structure determination
  - Structural alignment of host 2H phosphoesterases using DALI
  - Thin-layer chromatography
  - High performance liquid chromatography (HPLC)
  - Viral 2H phosphoesterase dendrogram
  - Construction of mutant phage
  - Phage challenge assays
- QUANTIFICATION AND STATISTICAL ANALYSIS

SUPPLEMENTAL INFORMATION

Supplemental information can be found online at https://doi.org/10.1016/j.cell.2024.07.057.

ACKNOWLEDGMENTS

The authors are grateful to members of the Kranzusch lab for helpful comments and discussion. The work was funded by grants to P.J.K. from the Pew Biomedical Scholars program, the Burroughs Wellcome Fund PATH program, the Richard and Susan Smith Family Foundation, The Mathers Foundation, The Mark Foundation for Cancer Research, the Cancer Research Institute, the Parker Institute for Cancer Immunotherapy, the DFCI-Novartis Drug Discovery Program, and the National Institutes of Health (1DP2GM146250-01). J.A.D. is an investigator of the Howard Hughes Medical Institute (HHMI); research in the Doudna lab is supported by the HHMI, NIH/NIAID (U19AI171110, U54AI170792, U19AI135990, UH3AI150552, U01AI142817), NIH/NINDS (U19NS132303), NIH/NHLBI (R21HL173710), NSF (2334028), DOE (DE-AC02-05CH11231, 2553571, B656358), Lawrence Livermore National Laboratory, Apple Tree Partners (24180), UCB-Hampton University Summer Program, Mr. Li Ka Shing, Koret-Berkeley-TAU, Emerson Collective, the Gladstone Institutes, and the Innovate Genomics Institute (IGI). S.J.H. is supported through a Cancer Research Institute Irvington Postdoctoral Fellowship (CRI3996). J.N. was supported by funding from the Gladstone Institutes. This research was supported by an agreement between the Advanced Photon Source, a U.S. Department of Energy (DOE) Office of Science user facility operated for the DOE Office of Science by Argonne National Laboratory under contract no. DE-AC02-06CH11357, and the Diamond Light Source, the U.K.'s national synchrotron science facility, located at the Harwell Science and Innovation Campus in Oxfordshire, where the work was performed under proposal GUP-83228. Parts of this research was conducted on the Wynton Cluster at the University of California, San Francisco (UCSF) and supported by UCSF IT.

AUTHOR CONTRIBUTIONS

Experiments were designed and conceived by S.J.H. and P.J.K. J.N. and J.A.D. performed computational structural prediction analyses and the initial identification of phage Acb1 structural homologs. S.J.H. determined the poxvirus cGAMP PDE structures and performed all biochemical and phage experiments. The manuscript was written by S.J.H. and P.J.K. All authors contributed to editing the manuscript and supporting the conclusions.

DECLARATION OF INTERESTS

J.A.D. is a co-founder of Caribou Biosciences, Editas Medicine, Scribe Therapeutics, Intellia Therapeutics, and Mammoth Biosciences. J.A.D. is a scientific advisory board member of Vertex, Caribou Biosciences, Intellia Therapeutics, Scribe Therapeutics, Mammoth Biosciences, Algen Biotechnologies, Felix Biosciences, The Column Group, and Inari Agriculture. J.A.D. is Chief Science Advisor to Sixth Street, a Director at Johnson & Johnson, and Altos and Tempus and has research projects sponsored by Apple Tree Partners and Roche.

Received: April 29, 2024
Revised: July 5, 2024
Accepted: July 30, 2024
Published: August 27, 2024

REFERENCES

1. Wein, T., and Sorek, R. (2022). Bacterial origins of human cell-autonomous innate immune mechanisms. Nat. Rev. Immunol. *22*, 629–638. https://doi.org/10.1038/s41577-022-00705-4.
2. Slavik, K.M., and Kranzusch, P.J. (2023). CBASS to cGAS-STING: the origins and mechanisms of nucleotide second messenger immune signaling. Annu. Rev. Virol. *10*, 423–453. https://doi.org/10.1146/annurev-virology-111821-115636.
3. Ledvina, H.E., and Whiteley, A.T. (2024). Conservation and similarity of bacterial and eukaryotic innate immunity. Nat. Rev. Microbiol. *22*, 420–434. https://doi.org/10.1038/s41579-024-01017-1.
4. Whiteley, A.T., Eaglesham, J.B., de Oliveira Mann, C.C., Morehouse, B.R., Lowey, B., Nieminen, E.A., Danilchanka, O., King, D.S., Lee, A.S.Y., Mekalanos, J.J., et al. (2019). Bacterial cGAS-like enzymes synthesize diverse nucleotide signals. Nature *567*, 194–199. https://doi.org/10.1038/s41586-019-0953-5.
5. Cohen, D., Melamed, S., Millman, A., Shulman, G., Oppenheimer-Shaanan, Y., Kacen, A., Doron, S., Amitai, G., and Sorek, R. (2019). Cyclic GMP-AMP signalling protects bacteria against viral infection. Nature *574*, 691–695. https://doi.org/10.1038/s41586-019-1605-5.
6. Morehouse, B.R., Govande, A.A., Millman, A., Keszei, A.F.A., Lowey, B., Ofir, G., Shao, S., Sorek, R., and Kranzusch, P.J. (2020). STING cyclic dinucleotide sensing originated in bacteria. Nature *586*, 429–433. https://doi.org/10.1038/s41586-020-2719-5.
7. Sun, L., Wu, J., Du, F., Chen, X., and Chen, Z.J. (2013). Cyclic GMP-AMP synthase is a cytosolic DNA sensor that activates the type I interferon pathway. Science *339*, 786–791. https://doi.org/10.1126/science.1232458.
8. Gao, P., Ascano, M., Wu, Y., Barchet, W., Gaffney, B.L., Zillinger, T., Serganov, A.A., Liu, Y., Jones, R.A., Hartmann, G., et al. (2013). Cyclic [G(2',5')pA(3',5')p] is the metazoan second messenger produced by DNA-activated cyclic GMP-AMP synthase. Cell *153*, 1094–1107. https://doi.org/10.1016/j.cell.2013.04.046.
9. Ablasser, A., Goldeck, M., Cavlar, T., Deimling, T., Witte, G., Röhl, I., Hopfner, K.P., Ludwig, J., and Hornung, V. (2013). cGAS produces a 2'-

5′-linked cyclic dinucleotide second messenger that activates STING. Nature *498*, 380–384. https://doi.org/10.1038/nature12306.

10. Diner, E.J., Burdette, D.L., Wilson, S.C., Monroe, K.M., Kellenberger, C.A., Hyodo, M., Hayakawa, Y., Hammond, M.C., and Vance, R.E. (2013). The innate immune DNA sensor cGAS produces a noncanonical cyclic dinucleotide that activates human STING. Cell Rep. *3*, 1355–1361. https://doi.org/10.1016/j.celrep.2013.05.009.
11. Li, Y., Slavik, K.M., Toyoda, H.C., Morehouse, B.R., de Oliveira Mann, C.C., Elek, A., Levy, S., Wang, Z., Mears, K.S., Liu, J., et al. (2023). cGLRs are a diverse family of pattern recognition receptors in innate immunity. Cell *186*, 3261–3276.e20. https://doi.org/10.1016/j.cell.2023.05.038.
12. Lowey, B., Whiteley, A.T., Keszei, A.F.A., Morehouse, B.R., Mathews, I.T., Antine, S.P., Cabrera, V.J., Kashin, D., Niemann, P., Jain, M., et al. (2020). CBASS immunity uses CARF-related effectors to sense 3′-5′- and 2′-5′-linked cyclic oligonucleotide signals and protect bacteria from phage infection. Cell *182*, 38–49.e17. https://doi.org/10.1016/j.cell.2020.05.019.
13. Ye, Q., Lau, R.K., Mathews, I.T., Birkholz, E.A., Watrous, J.D., Azimi, C.S., Pogliano, J., Jain, M., and Corbett, K.D. (2020). HORMA domain proteins and a Trip13-like ATPase regulate bacterial cGAS-like enzymes to mediate bacteriophage immunity. Mol. Cell *77*, 709–722.e7. https://doi.org/10.1016/j.molcel.2019.12.009.
14. Bernheim, A., Millman, A., Ofir, G., Meitav, G., Avraham, C., Shomar, H., Rosenberg, M.M., Tal, N., Melamed, S., Amitai, G., et al. (2021). Prokaryotic viperins produce diverse antiviral molecules. Nature *589*, 120–124. https://doi.org/10.1038/s41586-020-2762-2.
15. Kaur, G., Iyer, L.M., Burroughs, A.M., and Aravind, L. (2021). Bacterial death and TRADD-N domains help define novel apoptosis and immunity mechanisms shared by prokaryotes and metazoans. eLife *10*, e70394. https://doi.org/10.7554/eLife.70394.
16. Johnson, A.G., Wein, T., Mayer, M.L., Duncan-Lowey, B., Yirmiya, E., Oppenheimer-Shaanan, Y., Amitai, G., Sorek, R., and Kranzusch, P.J. (2022). Bacterial gasdermins reveal an ancient mechanism of cell death. Science *375*, 221–225. https://doi.org/10.1126/science.abj8432.
17. Kibby, E.M., Conte, A.N., Burroughs, A.M., Nagy, T.A., Vargas, J.A., Whalen, L.A., Aravind, L., and Whiteley, A.T. (2023). Bacterial NLR-related proteins protect against phage. Cell *186*, 2410–2424.e18. https://doi.org/10.1016/j.cell.2023.04.015.
18. Wein, T., Johnson, A.G., Millman, A., Lange, K., Yirmiya, E., Hadary, R., Garb, J., Steinruecke, F., Hill, A.B., Kranzusch, P.J., et al. (2023). CARD-like domains mediate anti-phage defense in bacterial gasdermin systems. Preprint at bioRxiv. https://doi.org/10.1101/2023.05.28.542683.
19. Salimi Alizei, E., Hofmann, M., Thimme, R., and Neumann-Haefelin, C. (2021). Mutational escape from cellular immunity in viral hepatitis: variations on a theme. Curr. Opin. Virol. *50*, 110–118. https://doi.org/10.1016/j.coviro.2021.08.002.
20. Koonin, E.V., Dolja, V.V., and Krupovic, M. (2022). The logic of virus evolution. Cell Host Microbe *30*, 917–929. https://doi.org/10.1016/j.chom.2022.06.008.
21. Koonin, E.V., Makarova, K.S., Wolf, Y.I., and Krupovic, M. (2020). Evolutionary entanglement of mobile genetic elements and host defence systems: guns for hire. Nat. Rev. Genet. *21*, 119–131. https://doi.org/10.1038/s41576-019-0172-9.
22. Crespo-Bellido, A., and Duffy, S. (2023). The how of counter-defense: viral evolution to combat host immunity. Curr. Opin. Microbiol. *74*, 102320. https://doi.org/10.1016/j.mib.2023.102320.
23. Leavitt, A., Yirmiya, E., Amitai, G., Lu, A., Garb, J., Herbst, E., Morehouse, B.R., Hobbs, S.J., Antine, S.P., Sun, Z.J., et al. (2022). Viruses inhibit TIR gcADPR signalling to overcome bacterial defence. Nature *611*, 326–331. https://doi.org/10.1038/s41586-022-05375-9.
24. Yirmiya, E., Leavitt, A., Lu, A., Ragucci, A.E., Avraham, C., Osterman, I., Garb, J., Antine, S.P., Mooney, S.E., Hobbs, S.J., et al. (2024). Phages overcome bacterial immunity via diverse anti-defence proteins. Nature *625*, 352–359. https://doi.org/10.1038/s41586-023-06869-w.
25. Huiting, E., Cao, X., Ren, J., Athukoralage, J.S., Luo, Z., Silas, S., An, N., Carion, H., Zhou, Y., Fraser, J.S., et al. (2023). Bacteriophages inhibit and evade cGAS-like immune function in bacteria. Cell *186*, 864–876.e21. https://doi.org/10.1016/j.cell.2022.12.041.
26. Li, D., Xiao, Y., Xiong, W., Fedorova, I., Wang, Y., Liu, X., Huiting, E., Ren, J., Gao, Z., Zhao, X., et al. (2023). Single phage proteins sequester TIR- and cGAS-generated signaling molecules. Preprint at bioRxiv. https://doi.org/10.1101/2023.11.15.567273.
27. Eaglesham, J.B., Pan, Y., Kupper, T.S., and Kranzusch, P.J. (2019). Viral and metazoan poxins are cGAMP-specific nucleases that restrict cGAS-STING signalling. Nature *566*, 259–263. https://doi.org/10.1038/s41586-019-0928-6.
28. Hobbs, S.J., Wein, T., Lu, A., Morehouse, B.R., Schnabel, J., Leavitt, A., Yirmiya, E., Sorek, R., and Kranzusch, P.J. (2022). Phage anti-CBASS and anti-Pycsar nucleases subvert bacterial immunity. Nature *605*, 522–526. https://doi.org/10.1038/s41586-022-04716-y.
29. Athukoralage, J.S., McMahon, S.A., Zhang, C., Grüschow, S., Graham, S., Krupovic, M., Whitaker, R.J., Gloster, T.M., and White, M.F. (2020). An anti-CRISPR viral ring nuclease subverts type III CRISPR immunity. Nature *577*, 572–575. https://doi.org/10.1038/s41586-019-1909-5.
30. Sanchez, E.L., and Lagunoff, M. (2015). Viral activation of cellular metabolism. Virology *479–480*, 609–618. https://doi.org/10.1016/j.virol.2015.02.038.
31. Daugherty, M.D., and Malik, H.S. (2012). Rules of engagement: molecular insights from host-virus arms races. Annu. Rev. Genet. *46*, 677–700. https://doi.org/10.1146/annurev-genet-110711-155522.
32. Hampton, H.G., Watson, B.N.J., and Fineran, P.C. (2020). The arms race between bacteria and their phage foes. Nature *577*, 327–336. https://doi.org/10.1038/s41586-019-1894-8.
33. Nomburg, J., Price, N., and Doudna, J.A. (2024). Birth of new protein folds and functions in the virome. Preprint at bioRxiv. https://doi.org/10.1101/2024.01.22.576744.
34. Offerman, K., Carulei, O., van der Walt, A.P., Douglass, N., and Williamson, A.L. (2014). The complete genome sequences of poxviruses isolated from a penguin and a pigeon in South Africa and comparison to other sequenced avipoxviruses. BMC Genomics *15*, 463. https://doi.org/10.1186/1471-2164-15-463.
35. Vennard, C., and Sintim, H.O. (2022). An expanding role of 2′,3′-cyclic nucleotide monophosphates in bacteria. ACS Cent. Sci. *8*, 1480–1483. https://doi.org/10.1021/acscentsci.2c01184.
36. Mitsutomi, S., Akimitsu, N., Sekimizu, K., and Kaito, C. (2019). Identification of 2H phosphoesterase superfamily proteins with 2′-CPDase activity. Biochimie *165*, 235–244. https://doi.org/10.1016/j.biochi.2019.08.008.
37. Shi, H., Wu, J., Chen, Z.J., and Chen, C. (2015). Molecular basis for the specific recognition of the metazoan cyclic GMP-AMP by the innate immune adaptor protein STING. Proc. Natl. Acad. Sci. USA *112*, 8947–8952. https://doi.org/10.1073/pnas.1507317112.
38. Kranzusch, P.J., Wilson, S.C., Lee, A.S.Y., Berger, J.M., Doudna, J.A., and Vance, R.E. (2015). Ancient origin of cGAS-STING reveals mechanism of universal 2′,3′ cGAMP signaling. Mol. Cell *59*, 891–903. https://doi.org/10.1016/j.molcel.2015.07.022.
39. Slavik, K.M., Morehouse, B.R., Ragucci, A.E., Zhou, W., Ai, X., Chen, Y., Li, L., Wei, Z., Bähre, H., König, M., et al. (2021). cGAS-like receptors sense RNA and control 3′2′-cGAMP signalling in Drosophila. Nature *597*, 109–113. https://doi.org/10.1038/s41586-021-03743-5.
40. Holleufer, A., Winther, K.G., Gad, H.H., Ai, X., Chen, Y., Li, L., Wei, Z., Deng, H., Liu, J., Frederiksen, N.A., et al. (2021). Two cGAS-like receptors induce antiviral immunity in Drosophila. Nature *597*, 114–118. https://doi.org/10.1038/s41586-021-03800-z.
41. Cai, H., Li, L., Slavik, K.M., Huang, J., Yin, T., Ai, X., Hédelin, L., Haas, G., Xiang, Z., Yang, Y., et al. (2023). The virus-induced cyclic dinucleotide 2′3′-c-di-GMP mediates STING-dependent antiviral immunity in

Drosophila. Immunity *56*, 1991–2005.e9. https://doi.org/10.1016/j.immuni.2023.08.006.

42. Lau, R.K., Ye, Q., Birkholz, E.A., Berg, K.R., Patel, L., Mathews, I.T., Watrous, J.D., Ego, K., Whiteley, A.T., Lowey, B., et al. (2020). Structure and mechanism of a cyclic trinucleotide-activated bacterial endonuclease mediating bacteriophage immunity. Mol. Cell *77*, 723–733.e6. https://doi.org/10.1016/j.molcel.2019.12.010.
43. Jenal, U., Reinders, A., and Lori, C. (2017). Cyclic di-GMP: second messenger extraordinaire. Nat. Rev. Microbiol. *15*, 271–284. https://doi.org/10.1038/nrmicro.2016.190.
44. Jakob, N.J., Müller, K., Bahr, U., and Darai, G. (2001). Analysis of the first complete DNA sequence of an invertebrate iridovirus: coding strategy of the genome of Chilo iridescent virus. Virology *286*, 182–196. https://doi.org/10.1006/viro.2001.0963.
45. Eaglesham, J.B., McCarty, K.L., and Kranzusch, P.J. (2020). Structures of diverse poxin cGAMP nucleases reveal a widespread role for cGAS-STING evasion in host-pathogen conflict. eLife *9*, e59753. https://doi.org/10.7554/eLife.59753.
46. Jenson, J.M., Li, T., Du, F., Ea, C.K., and Chen, Z.J. (2023). Ubiquitin-like conjugation by bacterial cGAS enhances anti-phage defence. Nature *616*, 326–331. https://doi.org/10.1038/s41586-023-05862-7.
47. Richmond-Buccola, D., Hobbs, S.J., Garcia, J.M., Toyoda, H., Gao, J., Shao, S., Lee, A.S.Y., and Kranzusch, P.J. (2024). A large-scale type I CBASS antiphage screen identifies the phage prohead protease as a key determinant of immune activation and evasion. Cell Host Microbe *32*, 1074–1088.e5. https://doi.org/10.1016/j.chom.2024.05.021.
48. Duncan-Lowey, B., McNamara-Bordewick, N.K., Tal, N., Sorek, R., and Kranzusch, P.J. (2021). Effector-mediated membrane disruption controls cell death in CBASS antiphage defense. Mol. Cell *81*, 5039–5051.e5. https://doi.org/10.1016/j.molcel.2021.10.020.
49. Mazumder, R., Iyer, L.M., Vasudevan, S., and Aravind, L. (2002). Detection of novel members, structure-function analysis and evolutionary classification of the 2H phosphoesterase superfamily. Nucleic Acids Res. *30*, 5229–5243. https://doi.org/10.1093/nar/gkf645.
50. Thornbrough, J.M., Jha, B.K., Yount, B., Goldstein, S.A., Li, Y., Elliott, R., Sims, A.C., Baric, R.S., Silverman, R.H., and Weiss, S.R. (2016). Middle East respiratory syndrome coronavirus NS4b protein inhibits Host RNase L Activation. mBio *7*, e00258. https://doi.org/10.1128/mBio.00258-16.
51. Sui, B., Huang, J., Jha, B.K., Yin, P., Zhou, M., Fu, Z.F., Silverman, R.H., Weiss, S.R., Peng, G., and Zhao, L. (2016). Crystal structure of the mouse hepatitis virus ns2 phosphodiesterase domain that antagonizes RNase L activation. J. Gen. Virol. *97*, 880–886. https://doi.org/10.1099/jgv.0.000395.
52. Brandmann, T., and Jinek, M. (2015). Crystal structure of the C-terminal 2′,5′-phosphodiesterase domain of group A rotavirus protein VP3. Proteins *83*, 997–1002. https://doi.org/10.1002/prot.24794.
53. Goldstein, S.A., and Elde, N.C. (2024). Recurrent viral capture of cellular phosphodiesterases that antagonize OAS-RNase L. Proc. Natl. Acad. Sci. USA *121*, e2312691121. https://doi.org/10.1073/pnas.2312691121.
54. Myllykoski, M., and Kursula, P. (2017). Structural aspects of nucleotide ligand binding by a bacterial 2H phosphoesterase. PLoS One *12*, e0170355. https://doi.org/10.1371/journal.pone.0170355.
55. Remus, B.S., Jacewicz, A., and Shuman, S. (2014). Structure and mechanism of E. coli RNA 2′,3′-cyclic phosphodiesterase. RNA *20*, 1697–1705. https://doi.org/10.1261/rna.046797.114.
56. Kozlov, G., Lee, J., Elias, D., Gravel, M., Gutierrez, P., Ekiel, I., Braun, P.E., and Gehring, K. (2003). Structural evidence that brain cyclic nucleotide phosphodiesterase is a member of the 2H phosphodiesterase superfamily. J. Biol. Chem. *278*, 46021–46028. https://doi.org/10.1074/jbc.M305176200.
57. Jumper, J., Evans, R., Pritzel, A., Green, T., Figurnov, M., Ronneberger, O., Tunyasuvunakool, K., Bates, R., Žídek, A., Potapenko, A., et al. (2021). Highly accurate protein structure prediction with AlphaFold. Nature *596*, 583–589. https://doi.org/10.1038/s41586-021-03819-2.
58. Baek, M., DiMaio, F., Anishchenko, I., Dauparas, J., Ovchinnikov, S., Lee, G.R., Wang, J., Cong, Q., Kinch, L.N., Schaeffer, R.D., et al. (2021). Accurate prediction of protein structures and interactions using a three-track neural network. Science *373*, 871–876. https://doi.org/10.1126/science.abj8754.
59. Sayers, E.W., Bolton, E.E., Brister, J.R., Canese, K., Chan, J., Comeau, D.C., Connor, R., Funk, K., Kelly, C., Kim, S., et al. (2022). Database resources of the national center for biotechnology information. Nucleic Acids Res. *50*, D20–D26. https://doi.org/10.1093/nar/gkab1112.
60. Chen, I.A., Chu, K., Palaniappan, K., Ratner, A., Huang, J., Huntemann, M., Hajek, P., Ritter, S.J., Webb, C., Wu, D., et al. (2023). The IMG/M data management and analysis system v.7: content updates and new features. Nucleic Acids Res. *51*, D723–D732. https://doi.org/10.1093/nar/gkac976.
61. Liebschner, D., Afonine, P.V., Baker, M.L., Bunkóczi, G., Chen, V.B., Croll, T.I., Hintze, B., Hung, L.W., Jain, S., McCoy, A.J., et al. (2019). Macromolecular structure determination using X-rays, neutrons and electrons: recent developments in Phenix. Acta Crystallogr. D Struct. Biol. *75*, 861–877. https://doi.org/10.1107/S2059798319011471.
62. Emsley, P., Lohkamp, B., Scott, W.G., and Cowtan, K. (2010). Features and development of coot. Acta Crystallogr. D Biol. Crystallogr. *66*, 486–501. https://doi.org/10.1107/S0907444910007493.
63. Mirdita, M., Schütze, K., Moriwaki, Y., Heo, L., Ovchinnikov, S., and Steinegger, M. (2022). ColabFold: making protein folding accessible to all. Nat. Methods *19*, 679–682. https://doi.org/10.1038/s41592-022-01488-1.
64. Holm, L., Laiho, A., Törönen, P., and Salgado, M. (2023). DALI shines a light on remote homologs: one hundred discoveries. Protein Sci. *32*, e4519. https://doi.org/10.1002/pro.4519.
65. Zhou, W., Whiteley, A.T., de Oliveira Mann, C.C., Morehouse, B.R., Nowak, R.P., Fischer, E.S., Gray, N.S., Mekalanos, J.J., and Kranzusch, P.J. (2018). Structure of the human cGAS-DNA complex reveals enhanced control of immune surveillance. Cell *174*, 300–311.e11. https://doi.org/10.1016/j.cell.2018.06.026.
66. Vonrhein, C., Flensburg, C., Keller, P., Sharff, A., Smart, O., Paciorek, W., Womack, T., and Bricogne, G. (2011). Data processing and analysis with the autoPROC toolbox. Acta Crystallogr. D Biol. Crystallogr. *67*, 293–302. https://doi.org/10.1107/S0907444911007773.
67. McCoy, A.J., Grosse-Kunstleve, R.W., Adams, P.D., Winn, M.D., Storoni, L.C., and Read, R.J. (2007). Phaser crystallographic software. J. Appl. Crystallogr. *40*, 658–674. https://doi.org/10.1107/S0021889807021206.
68. Letunic, I., and Bork, P. (2021). Interactive Tree Of Life (iTOL) v5: an online tool for phylogenetic tree display and annotation. Nucleic Acids Res. *49*, W293–W296. https://doi.org/10.1093/nar/gkab301.
69. Adler, B.A., Hessler, T., Cress, B.F., Lahiri, A., Mutalik, V.K., Barrangou, R., Banfield, J., and Doudna, J.A. (2022). Broad-spectrum CRISPR-Cas13a enables efficient phage genome editing. Nat. Microbiol. *7*, 1967–1979. https://doi.org/10.1038/s41564-022-01258-x.

STAR★METHODS

KEY RESOURCES TABLE

REAGENT or RESOURCE	SOURCE	IDENTIFIER
Bacterial and virus strains		
E. coli BL21-DE3 RIL	Agilent	230245
E. coli MG1655	ATCC	700926
E. coli TOP 10	Invitrogen	C404052
Escherichia phage T4 Δacb2	This paper	N/A
Escherichia phage T4 Δacb1/Δacb2	This paper	N/A
Chemicals, peptides, and recombinant proteins		
Ni-NTA Agarose	Qiagen	30250
Quick CIP	New England Biolabs	M0525S
PEI-Cellulose F TLC plate	EMD Biosciences	EM1.05579.0001
HiLoad 16/600 Superdex 75 pg Column	Cytiva	28989333
ATP, [α-32P], 3000 Ci/mmol 10 mCi/ml	Perkin Elmer	BLU003H250UC
ATP, GTP, CTP, UTP	New England Biolabs	N0450S
2′3′-cGG	Biolog Life Science Institute	C 182
2′3′-cGAMP	Biolog Life Science Institute	C 161
3′3′-cGAMP	Biolog Life Science Institute	C 117
3′2′-cGAMP	Biolog Life Science Institute	C 238
3′3′-cGG	Biolog Life Science Institute	C 057
3′3′-cAA	Biolog Life Science Institute	C 088
3′3′3′-cAAA	Biolog Life Science Institute	C 362
Non-hydrolyzable 2′3′-cGAMP	Biolog Life Science Institute	Set 101
Deposited data		
Penguinpox cGAMP PDE	This paper	PDB: 9BKQ
Penguinpox cGAMP PDE H72A	This paper	PDB: 9CIW
Recombinant DNA		
Plasmid DNA for expression of recombinant cGAMP PDE	This paper	See Table S2
Plasmid DNA to generate recombinant T4 phages	This paper	See Table S2
Software and algorithms		
Phenix 1.21-5207	Liebschner et al.[61]	https://www.phenixonline.org/
Coot 0.8.9	Emsley and Cowtan[62]	https://www2.mrclmb.cam.ac.uk/personal/pemsley/coot/
PyMOL (v 2.4.2)	Schrödinger, LLC	https://pymol.org/
Colabfold	Mirdita et al.[63]	https://colab.research.google.com/github/sokrypton/ColabFold/blob/main/AlphaFold2.ipynb
DALI	Holm et al.[64]	http://ekhidna2.biocenter.helsinki.fi/dali/
Python to generate dendrogram	This paper	https://github.com/jnoms/2024_Hobbs_et_al_dendrogram

RESOURCE AVAILABILITY

Lead contact

Further information and requests for resources and reagents should be directed to and will be fulfilled by the lead contact, Philip Kranzusch (philip_kranzusch@dfci.harvard.edu).

Materials availability

This study did not generate new unique reagents.

Data and code availability

- Coordinates of the penguinpox cGAMP PDE structure are publicly available in the Protein Data Bank under the accession number: 9BKQ and 9CIW
- All code used in this manuscript is publicly available at https://github.com/jnoms/2024_Hobbs_et_al_dendrogram
- Any additional information required to reanalyze the data reported in this paper is available from the lead contact upon request.

EXPERIMENTAL MODEL AND STUDY PARTICIPANT DETAILS

Bacterial cell lines used in this study include Top10 *E. coli* cells grown at 37°C in LB media for routine cloning. For protein expression, BL21(DE3)-RIL cells (Agilent) were grown at 37°C and expression was induced by addition of 0.5 mM IPTG at 16°C for ~16 hours. For phage challenge assays, *E. coli* MG1655 (ATCC) were transformed with plasmids encoding WT or inactivated CBASS operons and plaque assays were performed at 30°C.

METHOD DETAILS

Cloning and plasmid construction

The protein sequence of peguinpox cGAMP PDE (gp029, YP_009046028.1) was codon optimized for *E. coli* and synthesized as gBlocks (Integrated DNA Technologies) with ~20 base pairs of homology flanking the insert sequence and cloned into a custom pET-SUMO2 vector by Gibson assembly.[65] Mutations were introduced by overlapping PCR using the wild type cGAMP PDE plasmid as a template. All plasmids were transformed into the *E. coli* strain Top10 (Invitrogen) and grown in LB media supplemented with Ampicillin (100 μg mL^{-1}) for routine cloning.

Protein expression and purification

Expression plasmids encoding 6×His-SUMO2-penguinpox cGAMP PDE (gp029) were transformed into *E. coli* strain BL21-RIL (Agilent) and grown as overnight cultures in ~30 mL of MDG media at 37°C with 230 RPM shaking. Overnight MDG cultures were used to inoculate 1–2 L M9ZB cultures which were grown at 37°C until OD_{600} reached 1.5, then induced with 0.5 mM IPTG and incubated overnight at 16°C with 230 RPM shaking. Bacterial pellets were resuspended and sonicated in lysis buffer (20 mM HEPES-KOH pH 7.5, 400 mM NaCl, 30 mM imidazole, 10% glycerol and 1 mM DTT), clarified by centrifugation at 3,200 × g for 15 minutes at 4°C and recombinant proteins were purified from the supernatant by running the clarified lysate over 4 mL (1 L cultures) or 8 mL (2 L cultures) of Ni-NTA resin (Qiagen) twice using gravity filtration. The Ni-NTA resin was washed with 20 mL lysis buffer, 50 mL wash buffer (20 mM HEPES-KOH pH 7.5, 1 M NaCl, 30 mM imidazole, 10% glycerol and 1 mM DTT), and 20 mL lysis buffer. Protein was eluted in elution buffer (20 mM HEPES-KOH pH 7.5, 400 mM NaCl, 300 mM imidazole, 10% glycerol and 1 mM DTT) and dialyzed overnight at 4°C into gel filtration buffer (20 mM HEPES-KOH pH 7.5, 250 mM KCl, 1 mM TCEP and 10% glycerol) using 20-kDa molecular weight cut-off spin column (Amicon). The 6×His-SUMO2 was removed by addition of ~250 μg human SENP2 protease (D364–L589, M497A) during dialysis. For biochemical studies using point mutants, recombinant proteins were concentrated to >10 mg mL^{-1}, aliquoted and flash frozen in LiN_2 after dialysis, and sample purity was analyzed by SDS–PAGE followed by Coomassie staining. For crystallization of wild type penguinpox cGAMP PDE, proteins were further purified by size exclusion chromatography using a 16/600 Superdex 75 column and gel filtration buffer. Pooled fractions were concentrated to 100 mg mL^{-1} and flash frozen in LiN_2.

Crystallization and structure determination

Crystals of the WT or H72A penguinpox cGAMP PDE–2′3′-cGAMP complex were grown at 18°C for 2 days using hanging-drop vapor diffusion. Purified WT or H72A cGAMP PDE protein was diluted to 10 mg mL^{-1} in a buffer containing 20 mM HEPES-KOH pH 7.5, 70 mM KCl, 1 mM TCEP and WT protein was incubated with 100 μM a phosphorothioate analog of 2′3′-cGAMP (Biolog Cat. No Set 101) and H72A protein was incubated with 100 μM of 2′3′-cGAMP (Biolog Cat. No C161) on ice for 20 minutes before crystallization screening. Initial screens were performed in 96-well trays with 70 μL reservoir solution by mixing 200 nL of protein mixture and 200 nL of reservoir solution using a Mosquito instrument (SPT Labtech). Initial hits were further optimized in EasyXtal 15-well trays (NeXtal Biotechnologies) with 400 μL reservoir solution and 2 μL drops set with a ratio of 1 μL of protein solution and 1 μL of reservoir solution. Optimized crystallization conditions were: 200 mM magnesium formate and 24% (w/v) PEG 3350 (Sigma). The crystal was cryo-protected by dipping the crystal in a 1 μL drop of reservoir solution supplemented with 20% glycerol before harvesting with a 0.2 μm nylon loop. X-ray diffraction data were collected at the Diamond Light Source MX beamline. Data were processed using autoProc.[66] Experimental phase information for poxvirus cGAMP PDE was determined by molecular replacement using Phaser and a starting model predicted by AlphaFold2.[57,67] Structural modelling was completed in Coot and refined with PHENIX.[61,62] Final

structures were refined to stereochemistry statistics as reported in Table S1. All structural figures were generated with PyMOL (The PyMOL Molecular Graphics System, version 2.4.2, Schrödinger, LLC).

Structural alignment of host 2H phosphoesterases using DALI

Structural alignments were performed using the DALI server with pairwise alignment of either ligand-bound penguinpox cGAMP PDE (chain A) or ligand-bound phage Acb1 (PDB 7T27) against the full PDB.[64]

Thin-layer chromatography

Thin-layer chromatography was used to analyze degradation of nucleotide immune signals as described previously.[27,28] Synthesis of 2′3′-cGAMP was performed in reaction buffer consisting of 2 μM 50 mM recombinant cGAS from *Mus musculus*, Tris-HCl pH 7.5, 25 μM ATP, 25 μM GTP, trace amounts of α-32P-labelled GTP, 100 mM KCl, 1 mM dithiothreitol (DTT), 5 mM MgCl2, 1 mM $MnCl_2$, and 1 μM 45 bp stimulatory dsDNA.[65] Synthesis of 3′3′-cGAMP was performed in reaction buffer consisting of 2 μM 50 mM recombinant DncV from *Vibrio cholerae*, 50 mM Tris-HCl pH 7.5, 25 μM ATP, 25 μM GTP, trace amounts of α-32P-labelled GTP, 100 mM KCl, 1 mM dithiothreitol (DTT), and 5 mM $MgCl_2$.[4] Reactions were performed in a volume of 25 μL and incubated at 37°C for 16 hours. Unincorporated NTPs were digested by adding 0.5 μL Quick CIP (NEB) and incubation at 37°C for 30 minutes. Reactions were stored at −20°C and used as inputs for downstream degradation assays. To analyze degradation of 2′3′-cGAMP and 3′3′-cGAMP, 100 nM recombinant viral enzyme was added to reactions consisting of 50 mM Tris-HCl pH 7.5, 50 mM KCl, 1 mM DTT, and 0.2 μL cyclic dinucleotide synthesis reactions. Reactions were incubated at 37°C for 20 minutes and 0.5 μL was spotted onto a 20 cm x 20 cm PEI-cellulose thin-layer chromatography plate (Sigma) and run in 1.5 M KH_2PO_4 buffer (pH 3.8) for 1.5 hours. Plates were air-dried at room temperature and exposed to a phosphor screen for 2–4 hours before analysis on a Typhoon Trio Variable Mode Imager System (GE Healthcare).

High performance liquid chromatography (HPLC)

To analyze reaction products by HPLC, reactions were performed in a volume of 120 μL consisting of 50 mM Tris-HCl pH 7.5, 50 mM KCl, 1 mM DTT, and 12 μL of a 10× stock of recombinant viral enzyme (concentration indicated in figure legends). Reactions were incubated at 37°C for 30 minutes, heat inactivated at 95°C for 2 minutes, and filtered through 3 kDa cutoff filters (Millipore Sigma). The flow-through (30 μL) was transferred to a HPLC vial and analyzed using an Agilent 1260 Infinity II HPLC system with a 2.1 × 100 mm Zorbax SB-Aq column (Agilent) and a mobile phase A of water + 0.1% ammonium formate and a mobile phase B of methanol + 0.1% ammonium formate. The flow rate kept at 450 μL mL^{-1} consisting of a 1 minute hold at 0% B and increased to 100% B over 9 min. The column was at room temperature and an injection volume of 10 μL was used.

Viral 2H phosphoesterase dendrogram

DaliLite v5[64] was used to conduct all-by-all structural alignments of a panel of predicted and experimental structures. The accession numbers for the predicted protein sequences are: Phage T4, NP_049750; Marseillevirus, GenBank: YP_003406995; IIV-6, GenBank: NP_149590; Middle East Respiratory Syncitial virus (MERS), GenBank: YP_009047207; Penguinpox cGAMP PDE, GenBank: YP_009046028; Murine Hepatitis Virus, GenBank: YP_009824980; Porcine Torovirus, GenBank: YP_008798230; Rotavirus A, GenBank: YP_002302228; Phage RB16, GenBank: YP_003858481. Experimental structures were used for Penguinpox cGAMP PDE and Phage FBB1 Acb1. Structure predictions were used for all other proteins, with those generated by Nomburg et al. used where available,[33] or web-based Colabfold[63] used for structure prediction otherwise. In the case of Porcine Torovirus and Rotavirus A, only the 2H phosphoesterase region of the proteins were used for DALI alignments. Predicted structures were imported to DALI database files using the dali_format_inputs subcommand of SAT (https://github.com/jnoms/SAT). DALI alignments were conducted using dali_matrix.sh (https://github.com/jnoms/vpSAT/blob/main/bin/dali_matrix.sh), and output files were processed using the aln_parse_dali_-matrix subcommand of SAT. iToL[68] was used to visualize the unrooted DALI dendrogram, and R v4.0.3 was used to generate the Z-score similarity matrix figure. All code can be found here: https://github.com/jnoms/2024_Hobbs_et_al_dendrogram.

Construction of mutant phage

Mutant phage T4 were constructed using a Cas13-based selection strategy, as described previously.[69] Templates for homologous recombination to T4 *acb2* (NCBI gene name: *vs.4*, NP_049728.1) were designed to introduce a single base pair deletion at nucleotide position 22 of the *acb2*, resulting in multiple mutations and several premature stop codons at 19, 29, and 44. Approximately 100 bp of homology to the T4 genome was inserted on either side of the target sites and this template was cloned into the high copy number plasmid pGEM9zf (Promega) using Gibson assembly in Top10 (Thermo) *E. coli* cells. Cells carrying this plasmid were infected with either WT T4 or T4 Δ*acb1*[28] to generate mixed populations that carry a small number of T4 Δ*acb2* and T4 Δ*acb1*/Δ*acb2* phages that have undergone recombination. To select for recombinant phages, guide RNAs (gRNAs) were designed to target the WT *acb2* sequence at the site of the desired mutations. These gRNAs were cloned into vector pBA559, which carries the gRNA-guided CRISPR effector nuclease Cas13d as previously described.[69] The mixed population of phages from the pGEM9zf-HR infections was plated on bacterial lawns containing cells expressing pBA559-*acb2* and resulting plaques were picked and expanded in liquid cultures under continued selection. Three independent clones of mutant phages were plaque purified under three rounds of selection before PCR amplifying the *acb2* locus and confirming the insertion of the desired mutations by Sanger sequencing.

Phage challenge assays

To test the fitness of mutant T4 phages in the presence of cyclic nucleotide immune signaling, we transformed *E. coli* MG1655 cells with a plasmid encoding an arabinose-inducible CBASS operon from *Escherichia albertii* GTC 14781 previously demonstrated to defend against T4 Δ*acb1*.[47] Cells that encode either the WT CBASS operon or an inactive version where the 2TM effector gene has been removed were grown in LB at 37°C to an OD600 ~1.0. The bacterial lawn was initiated by mixing 250 μL cells with 4 mL melted top agar (0.6% agarose in LB) containing 0.04% arabinose. Cell lawns were incubated at room temperature for 1 hour to let the top agar solidify and to induce operon expression. High titer stocks of mutant T4 phages were serially diluted and plated on bacterial lawns of *E. coli* cells and allowed to dry for 15 min. Plates were then incubated at 30°C overnight and imaged using a ChemiDoc MP imager (BioRad).

QUANTIFICATION AND STATISTICAL ANALYSIS

Symbols in bar graphs represent independent replicates. Data are plotted with error bars representing the standard deviation (SD). Statistical tests are described in the figure legends.

CellPress

Supplemental figures

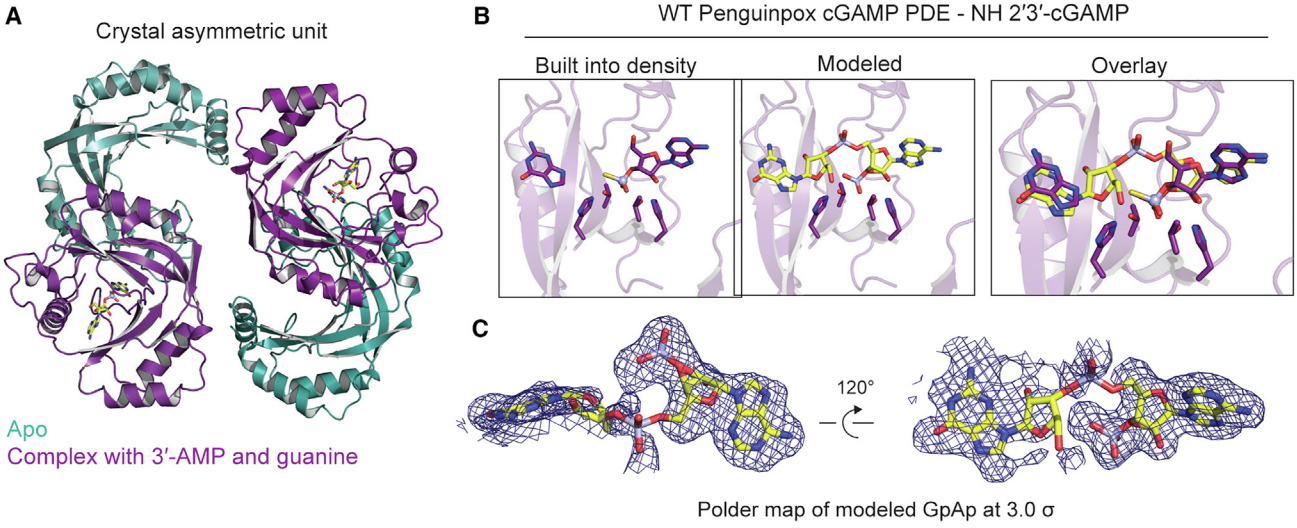

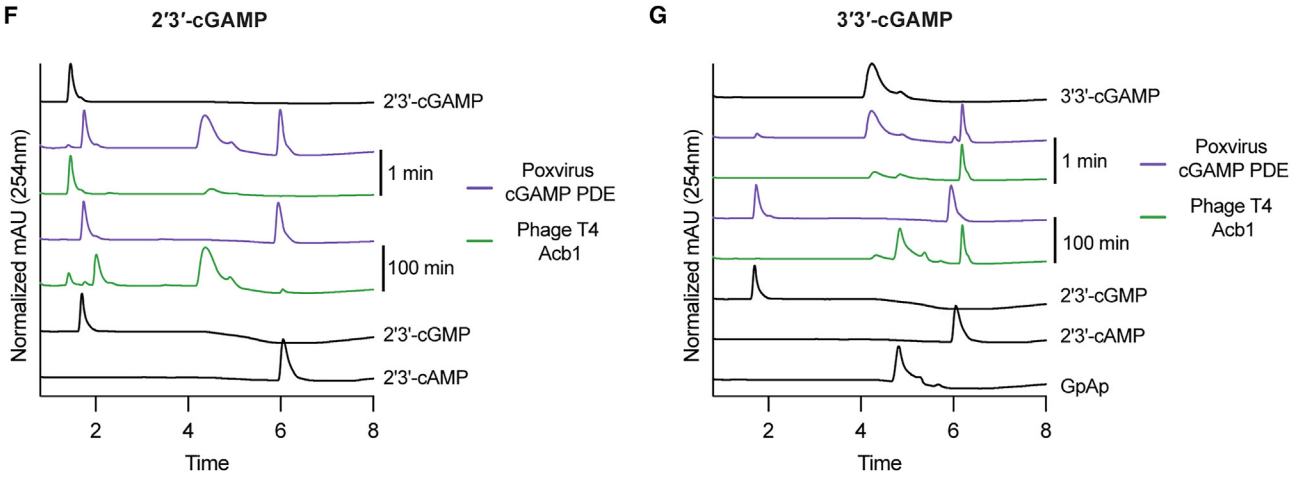

(legend on next page)

Figure S1. Structural and mechanistic analysis of poxvirus cGAMP PDE, related to Figure 1

(A) Cartoon representation of the proteins present in the crystal asymmetric unit.

(B) Detailed view of the ligands built into the active-site density for refinement and the modeled post-reaction product GpAp for comparison to phage Acb1-GpAp structures.

(C) Polder map of the modeled GpAp ligand contoured at 3.0 σ.

(D) Detailed view of the G[2′–5′]pA ligand built into the active site of H72A penguinpox cGAMP PDE.

(E) Polder map of the modeled G[2′–5′]pA ligand contoured at 4.0 σ.

(F) HPLC traces of chemical standards (black lines) or reaction products of 2′3′-cGAMP cleavage by poxvirus cGAMP PDE.

(G) HPLC traces of chemical standards (black lines) or reaction products of 3′3′-cGAMP cleavage by phage Acb1.

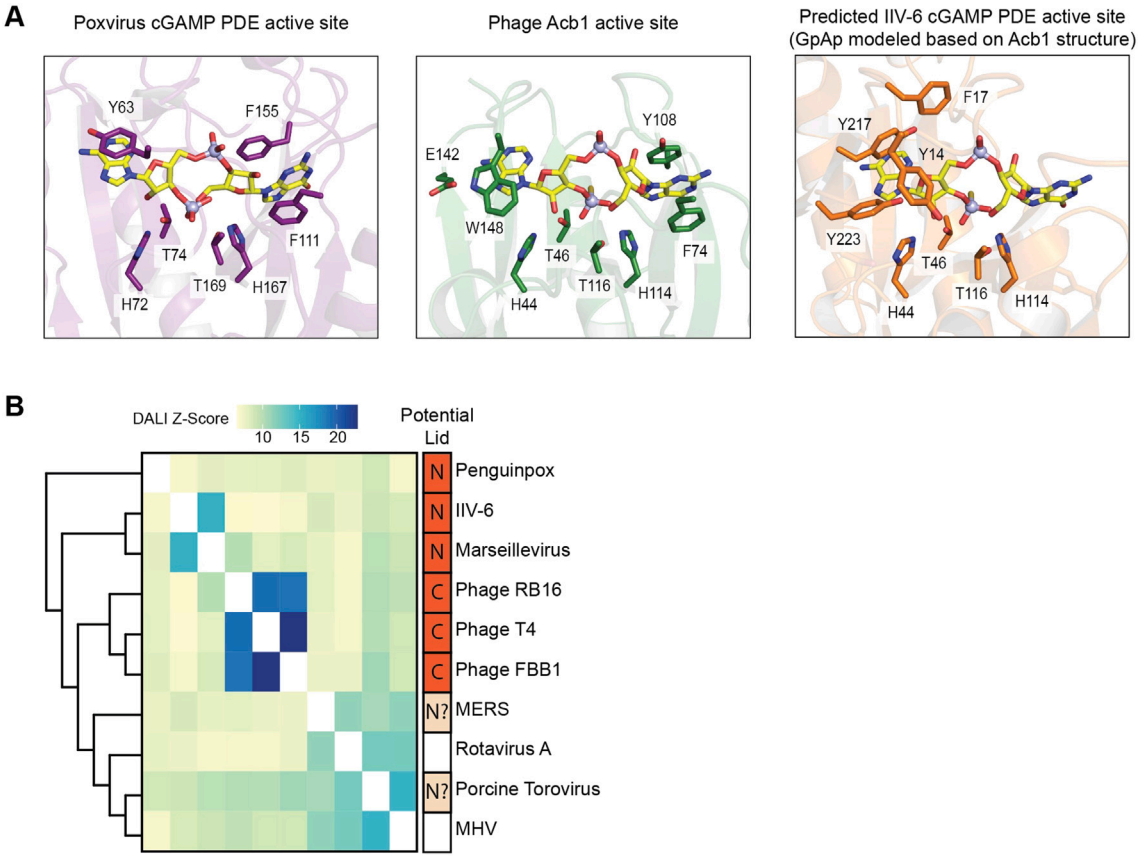

Figure S2. Structural analysis of diverse viral 2H phosphoesterase enzymes, related to Figure 3

(A) Detailed view of the residues involved ligand binding by poxvirus cGAMP PDE, phage FBB1 Acb1, or predicted equivalent residues in IIV-6 cGAMP PDE (AlphaFold prediction).

(B) Dendrogram based on DALI *Z* scores of the 2H phosphoesterase domain from the indicated virus. See methods for protein accession numbers.

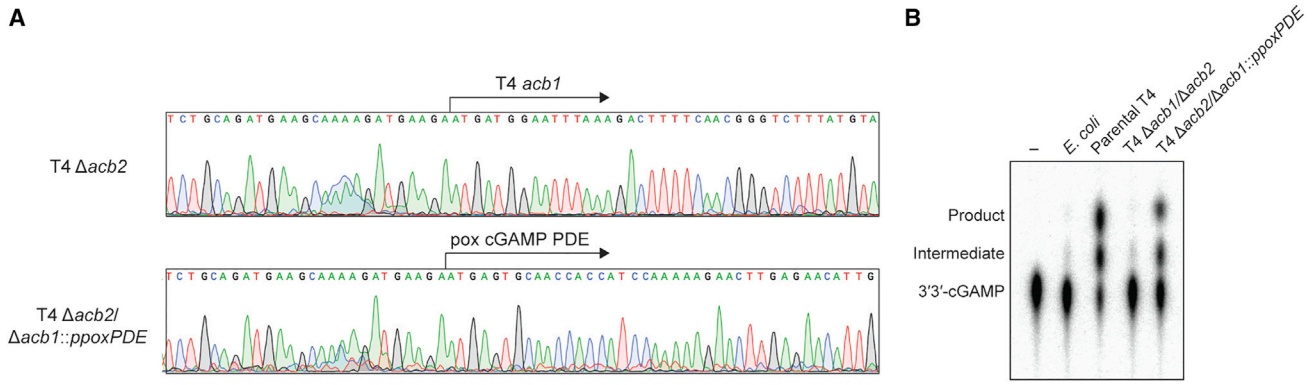

Figure S3. Analysis of eukaryotic cGAMP PDE substrate specificity and validation of mutant T4 phages, related to Figure 3

(A) Sanger sequencing confirming successful replacement of endogenous T4 *acb1* with penguinpox cGAMP PDE.

(B) Thin-layer chromatography analysis of the ability of phage-infected lysates to cleave radiolabeled 3′3′-cGAMP.